

Article

Multicomponent Comminution within a Stirred Media Mill and Its Application for Processing a Lithium-Ion Battery Slurry

Markus Nöske *, Jannes Müller, Christine Nowak, Kangqi Li, Xiaolu Xu, Sandra Breitung-Faes and Arno Kwade 

Institute for Particle Technology, TU Braunschweig, 38104 Braunschweig, Germany

* Correspondence: m.noeske@tu-bs.de; Tel.: +49-531-391-9624

Abstract: This study presents an approach for targeted comminution of component mixtures within a wet-operated stirred media mill. In the first step, a general understanding of the interactions between individual components on the grinding result with mixtures could be gained with basic experiments and following our former research work. In particular, a protective effect of the coarser particles on the fines could be elucidated. These findings were used to develop a process for the production of a battery slurry containing fine ground silicon particles as well as dispersed carbon black and graphite particles. By a tailored sample preparation applying a combination of particle dissolution and separation, the particle size distributions of carbon black and graphite particles were analyzed separately within the produced battery slurries. Based on the selective particle size analysis, the slurry preparation could be transferred from a complex multistage batch process using a dissolver to a stirred media mill, which was finally operated in a continuous one-passage mode. The prepared slurries were subsequently further processed to silicon-rich anodes using a pilot scale coating and drying plant. Afterward, the produced anodes were electrochemically characterized in full cells. The cell results prove a comparable electrochemical behavior of anode coatings derived from a dissolver- or mill-based slurry production process. Therefore, we could demonstrate that it is possible to integrate the mixing process for the production of multicomponent slurries into the comminution process for the preparation of individual materials upstream. Even with nearly identical starting sizes of their feed materials, the targeted particle size distributions of the single components can be reached, taking into account the different material-dependent particle strengths and sequential addition of single components to the multicomponent comminution process.

Keywords: multicomponent comminution; stirred media mill; battery slurry; silicon anode



Citation: Nöske, M.; Müller, J.; Nowak, C.; Li, K.; Xu, X.; Breitung-Faes, S.; Kwade, A. Multicomponent Comminution within a Stirred Media Mill and Its Application for Processing a Lithium-Ion Battery Slurry. *Processes* **2022**, *10*, 2309. <https://doi.org/10.3390/pr10112309>

Academic Editors: Weicheng Yan and Wangliang Li

Received: 16 October 2022

Accepted: 1 November 2022

Published: 6 November 2022

Publisher's Note: MDPI stays neutral with regard to jurisdictional claims in published maps and institutional affiliations.



Copyright: © 2022 by the authors. Licensee MDPI, Basel, Switzerland. This article is an open access article distributed under the terms and conditions of the Creative Commons Attribution (CC BY) license (<https://creativecommons.org/licenses/by/4.0/>).

1. Introduction

Real comminution and deagglomeration of single components, such as natural raw materials or synthetic aggregates, for the production of homogeneous dispersions, is a typical application for stirred media mills in industries such as the paint and coatings industry [1], the chemical and pharmaceutical industry [2], the food industry [3] or the electronic industry [4]. In contrast to this, the use of stirred media mills for the targeted comminution and processing of multicomponent systems is almost unexplored.

An example of such a multicomponent system containing different particulate components is a coating suspension used for the production of electrodes for lithium-ion batteries. Here, mainly electrochemical active materials such as metal oxides or graphite with particle sizes in the lower ten-micrometer range as well as other particulate additives, which increase, for example, the electrical conductivity or the porosity of the electrode coating (carbon blacks, graphite flakes, etc.) with particle sizes down to the submicron range, have to be homogeneously dispersed into binder solutions.

A current research topic in this context is the use of silicon as an active material on the anode side due to its high intrinsic storage capacity for lithium ions [5]. Several publications [6–8] have shown that the best anode performance can be achieved by using

silicon with a particle size in the lower submicron range ($x_{50,3} \approx 100\text{--}200$ nm). Thus, according to current knowledge, the production of fine silicon particles by means of fine wet grinding in stirred media mills of the industrial-grade polycrystalline feed material is described in the literature as a promising process for mass production [7–10].

After fine grinding, the silicon particles need to be finely dispersed downstream in a carbon-based matrix to ensure optimal utilization of the electrochemically active material during application [11]. Similar to the production of dispersion paints [12], the submicron silicon particles can subsequently be mixed with other particulate components and binders after fine grinding. Often a conductive additive such as carbon black must be deagglomerated, and a battery grade graphite needs to be mixed in. The latter provides the electrochemical storage capacity in addition to its function as a structure-forming coating filler. The machines used to produce these slurries are typically dissolvers or planetary mixers in batch mode and extruders for the continuous production of coating masses [13].

As a starting point of this work, a suitable water-based anode formulation based on the four-component system of silicon, carbon black, graphite, and binder were developed in a combined process using a stirred media mill and a dissolver. As a binder, a mixture of Na-CMC and SBR was used. In the first step, the silicon was ground in the mill, and then the finely ground silicon suspension was processed in a multistage batch process using a dissolver. This process was defined as the reference process for the following investigations.

Based on a developed general process understanding from basic results with quartz-limestone mixtures and following our former research work [14], the aim of this work was to transfer the suitable processing of the silicon-carbon black-graphite-binder mixture from the dissolver to a stirred media mill. Therefore, the complex, multistage batch process using the dissolver was transferred to only one continuous passage through the mill.

By using suitable sample preparation methods for the targeted dissolution or separation of individual components from the mixture, it was possible to carry out material-selective particle size analyses and, thus, to evaluate process parameters. In particular, the influence of different particle sizes of the individual components could be elucidated, and the novel process strategy of multicomponent comminution could be developed.

The results in this work show, for the first time, that it is possible to realize targeted processing of a multicomponent system by stirred media milling. Thus, in addition to former results with single components, defined particle size distributions can also be reached by the presented multicomponent comminution process. In addition to the battery slurry system studied, these results could be applicable to other industries such as the ceramic or paint industry when multicomponent formulations with fine ground particles are used for product manufacturing.

2. Materials and Methods

2.1. Materials

For the evaluation of different, component-specific feed particle sizes within a two-component grinding process, the materials quartz SF800 (Quarzwerte GmbH, Germany, $x_{50,3} = 2$ μm) and limestone Eskal300 (KSL Staubtechnik GmbH, Germany, $x_{50,3} = 2.1$ μm) were chosen as model materials following previous investigations [14]. In addition, the particle stabilization strategy, the solids concentration $c_{m,tot}$ with 0.3, as well as the sample preparation procedure for the selective particle size analysis, was kept constant for this water-based slurry system with respect to our former study [14]. For the realization of different feed sizes during the multicomponent comminution process, each particulate component was ground separately previous to the mixture process. During these, always 50:50 (m:m) mixtures of both components were ground with a constant slurry batch mass of 1–800 g (270 g quartz, 270 g limestone, 1260 g deion. water within the milling circuit). For a better comparison of particle strength values, the additional quartz grade SF300 (Quarzwerte GmbH, Germany, $x_{50,3} = 11$ μm) was also used.

The fine grinding process for the production of silicon nanoparticles was performed with the metallurgical silicon feed material from PyroPowders GmbH, Germany, ($x_{50,3} = \sim 20$ μm)

and by using an ethanolic formulation (absolute ethanol from Merck KGaA, Germany) with solids concentration $c_{m,tot}$ of 15 wt.% as well as an electrostatic stabilization approach by adding small amounts of sodium hydroxide (Merck KGaA, Germany) [15]. The production of the ground silicon particles was performed with a constant slurry batch mass of 1666.67 g (250 g silicon, 1416.67 g ethanol within the milling circuit).

For the production of battery slurries, the ground silicon suspensions were blended with deionized water (water:ethanol ratio of 3:2 (m:m)), a battery grade graphite ($x_{50,3} = 17 \mu\text{m}$), carbon black (Super C65 from Imerys S.A., France) and the two binders Na-CMC (Walocel 2000PA09 from Dow, Inc., USA) as well as SBR (BM451-B from Zeon Corporation, Japan). The final solids concentration $c_{m,tot}$ of the battery slurry, was adjusted to 0.26. In Table 1 the slurry recipe and the mass proportion of each component in the dry battery coating are summarized.

Table 1. Mass proportion of each component in the battery slurry and the dry battery coating.

Component	Description	Proportion in the Battery Slurry/wt.%	Proportion in the Dry Coating/wt.%
Silicon	Particulate component, active material	5.20	20.0
Carbon Black	Particulate component, conductivity coating additive	1.20	4.6
Graphite	Particulate component, active material	18.20	70.0
Na-CMC	Binder	0.94	3.6
SBR	Binder	0.47	1.8
Water	Solvent	44.53	0.0
Ethanol	Solvent	29.46	0.0

Within the reference, a process using a tooth disc dissolver for the battery slurry production, a total batch mass of 700 g, and during the sequential multicomponent grinding experiments, 4000 g slurry was produced.

2.2. Milling Setup

The horizontal stirred media mill Labstar from Netzsch-Feinmahltechnik GmbH, Germany, with a drive power of 3 kW and the Zeta grinding system was used for milling experiments. In the basic experiments for grinding the model materials quartz and limestone, a plastic-coated NElast stirrer was installed, and yttrium-stabilized zirconia grinding beads with a median size of $755 \mu\text{m}$ were chosen. For milling the battery materials silicon, carbon black, and graphite, the ceramic stirrer version Netzsch-Ceram C consisting of zirconia and the mixed oxide beads manufactured from zirconia and silicon oxide ($450 \mu\text{m}$) were selected. Both grinding media types were supplied by Sigmund Lindner GmbH, Germany. The mill was operated both in circular mode (see Figure 1) and in passage mode.

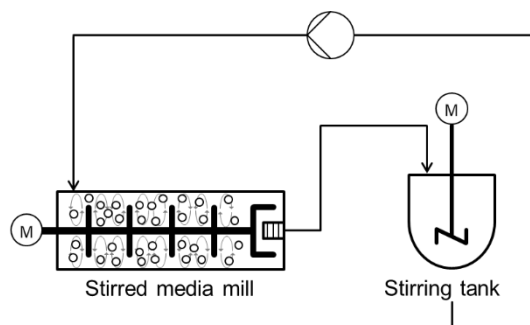


Figure 1. Milling setup for circuit mode operation used for the basic grinding investigations with quartz limestone mixtures and for the production of submicron silicon suspensions.

The double-walled, temperature-controlled grinding chamber was equipped with an inner lining of silicon carbide. For all grinding tests, a constant grinding media filling level of 80% of the active grinding chamber volume (540 mL) was set. Sampling was always performed directly behind the mill. The electrical power draw P during operation, as well as the no-load power draw P_0 directly after grinding and after emptying the mill, were measured. Thus, the specific energy input $E_{m,tot}$ could be calculated taking into account the solids mass flow of the product $\dot{m}_{P,tot}$ through the mill as well as the ground product mass $m_{P,tot}$. Equation (1) shows the formula used for the calculation of $E_{m,tot}$.

$$E_{m,tot} = \frac{(\bar{P} - P_0)}{m_{P,tot}} + \frac{\bar{P} - P_0}{\dot{m}_{P,tot}} \quad (1)$$

The first term of this equation takes into account the energy input during the circuit operation, and the second term takes into account the energy input that is added to the product during the last pass through the mill as sampling takes place directly after the mill and not out of the vessel.

In order to compare different parameters of a grinding process, Kwade developed the so-called stress energy model for stirred media mills [16]. He was able to show that process optimization is possible with the help of the so-called stress energy of the grinding media SE_{GM} .

$$SE \propto SE_{GM} = d_{GM}^3 \cdot v_t^2 \cdot \rho_{GM} \quad (2)$$

SE_{GM} can be understood as a measure of the real stress energy SE , which can only be described by a distribution based on real velocities within the mill. It describes the maximum kinetic energy of a single collision of the grinding media available for the comminution process. It depends on the diameter of the grinding media d_{GM} with the third power, on the stirrer tip speed v_t with the second power, and linearly on the density of the grinding media ρ_{GM} (see Equation (2)).

2.3. Setups for the Production of Battery Slurries

Within the reference process, the ground silicon suspension was further processed into a coating suspension by a multi-stage dispersion process using a toothed disc dissolver. Figure 2 schematically illustrates the setup used. During the dispersion within the dissolver, Dispermat CA 60 of the company VMA Getzmann GmbH, Germany, a toothed disk stirrer (diameter: 50 mm), was installed, as this is particularly suitable for deagglomeration tasks in addition to the pure mixture of the components. Here, a conductive carbon black (CB) was deagglomerated to the desired degree of deagglomeration, and the ground silicon particles, as well as battery graphite (Gr), were mixed into the suspension.

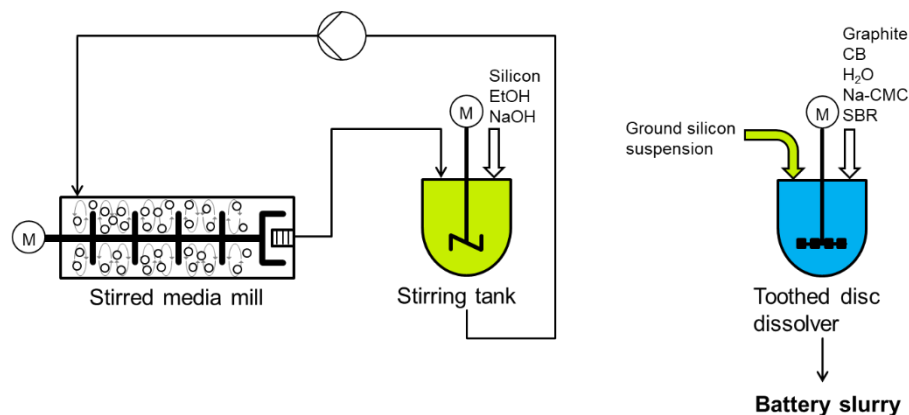


Figure 2. Setup for the production of a battery slurry by applying separate silicon grinding and dispersion of the other components.

Figure 3 shows the individual steps of the reference process. This process was started with the silicon grinding with the already described setup for the circuit grinding. The mill was operated with a stirrer tip speed v_t of $12 \text{ m}\cdot\text{s}^{-1}$. After the target particle size of the silicon (LD: $x_{50,3} = 200 \text{ nm}$; AS: $x_{50,3} = 120 \text{ nm}$) had been reached ($E_{m,tot} = 37 \text{ MJ}\cdot\text{kg}^{-1}$), the mill was emptied, and 8.4 g of carbon black was added to 243 g of the ground silicon suspension and pre-dispersed with the help of the toothed disc dissolver at a circumferential speed of $4 \text{ m}\cdot\text{s}^{-1}$ for 15 min (batch 1).

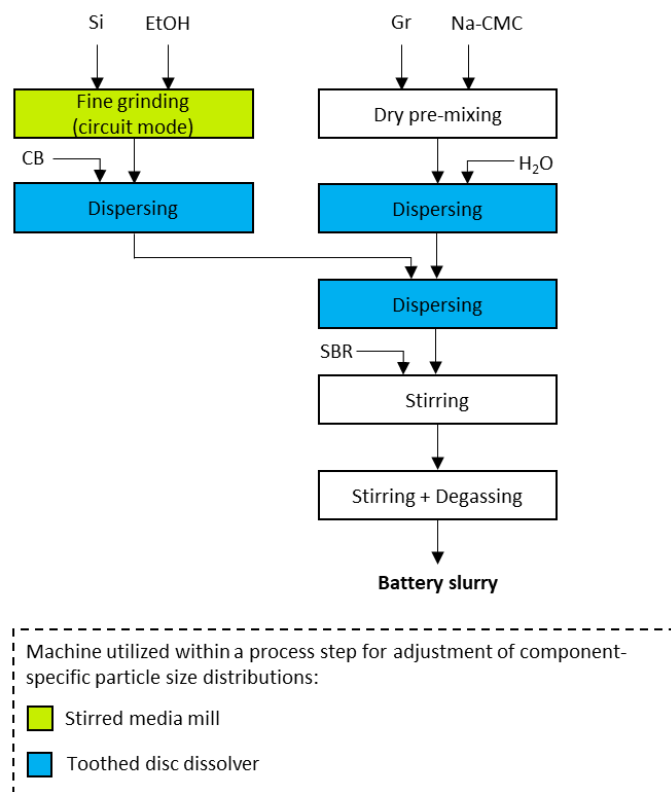


Figure 3. Process scheme for the production of battery slurries using the reference process within a tooth disc dissolver.

Parallel to this first batch, a second batch was prepared. For this, a dry premix containing 127.5 g graphite and 6.6 g Na-CMC was first prepared in a powder mixing step for 10 min using the Turbula T2F mixer from Willy A. Bachofen AG, Switzerland. This premix was then mixed into 312 g deionized water in a subsequent dispersion step using the toothed disc dissolver at a stirring speed of $9 \text{ m}\cdot\text{s}^{-1}$ for 30 min (batch 2).

In a further dispersion step with a stirring speed of $4 \text{ m}\cdot\text{s}^{-1}$, batch 1 was then added to batch 2 and homogenized for 15 min. Subsequently, a 3.3 g SBR binder was added, which was present as an emulsion with a solid mass concentration of $c_{m,tot} = 0.4$. A reduced stirring speed of $3 \text{ m}\cdot\text{s}^{-1}$ was selected for 10 min after the addition of SBR. Finally, the stirring speed was further reduced to $2.6 \text{ m}\cdot\text{s}^{-1}$, and the suspension was vacuum-degassed for 10 min. After this, the coating suspension was ready for further downstream processing into a reference electrode coating.

For the production of an electrode slurry using sequential milling within the stirred media mill, the periphery of the mill was extended according to Figure 4.

In addition to the previously used stirring tank for the silicon grinding in circuit mode (volume: 2 L), two further stirring tanks (volume: 6 L each), the associated tube connections as well, as 3-way ball valves for the passage operation of the mill were also installed.

After silicon grinding, 1391.5 g of the silicon suspension (with correspondingly 208 g of silicon) was used as the basis for further steps. For the next step, carbon black and Na-CMC, which had already been dry premixed for 10 min (Turbula T2F powder mixer

from Willy A. Bachofen AG, Switzerland), were first mixed into 1775.25 g deionized water. In total, 48 g carbon black and 36 g Na-CMC were always used.

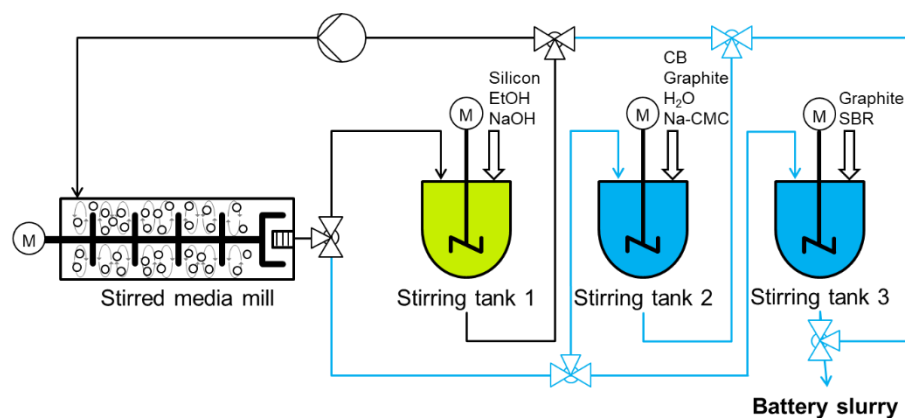


Figure 4. Setup for the sequential grinding of the mixture components for the production of a battery slurry.

Afterward, further milling of the mixture was then carried out, with one continuous passage or three pendulum passages between agitator vessels 2 and 3. The addition of 730.8 g graphite took place either before or after the last passage (see Figure 4). When added after the last passage, the graphite was suspended with the angled blade stirrer in the stirred tank 3 at a circumferential speed of $4 \text{ m}\cdot\text{s}^{-1}$ for 10 min. Finally, 18.6 g of the SBR binder was mixed into stirring tank 3 at a circumferential speed of $1.7 \text{ m}\cdot\text{s}^{-1}$ for 10 min. An overview of the three process variants investigated gives Figure 5. As stated before, the main differences between these process routes are:

1. Carbon black dispersing in 3-passage or single-passage mode
2. Addition of graphite before or after the last passage through the mill

Therefore, the first process variant, which uses three passages for the dispersing of the carbon black powder and includes the addition of the graphite before the last mill passage, was named “3 passage mode”. The other two processes use only one continuous passage through the mill and can be differentiated by the graphite addition, which takes place before (Conti-A) or after this mill passage (Conti-B).

2.4. Particle Size Analysis

Within this study, the particle size distributions of all suspension samples were analyzed by laser diffraction (LD) using the Mastersizer 3000 from Malvern Panalytical Ltd, United Kingdom. Additional investigations were carried out by acoustic spectroscopy (AS) for the analysis of silicon suspension samples with the device DT1200 from Quantachrome GmbH & Co. KG, Germany.

2.4.1. Selective Characterization of Quartz-Limestone Mixtures

In order to measure the particle size distributions from ground material mixtures separately for each component, the limestone particles were dissolved out of the quartz limestone mixture by the addition of hydrochloric acid. Due to a back calculation based on the particle size distribution of the mixture and remaining quartz, the distribution for the limestone particles could also be calculated. A detailed description of this procedure was given in our previous study [14].

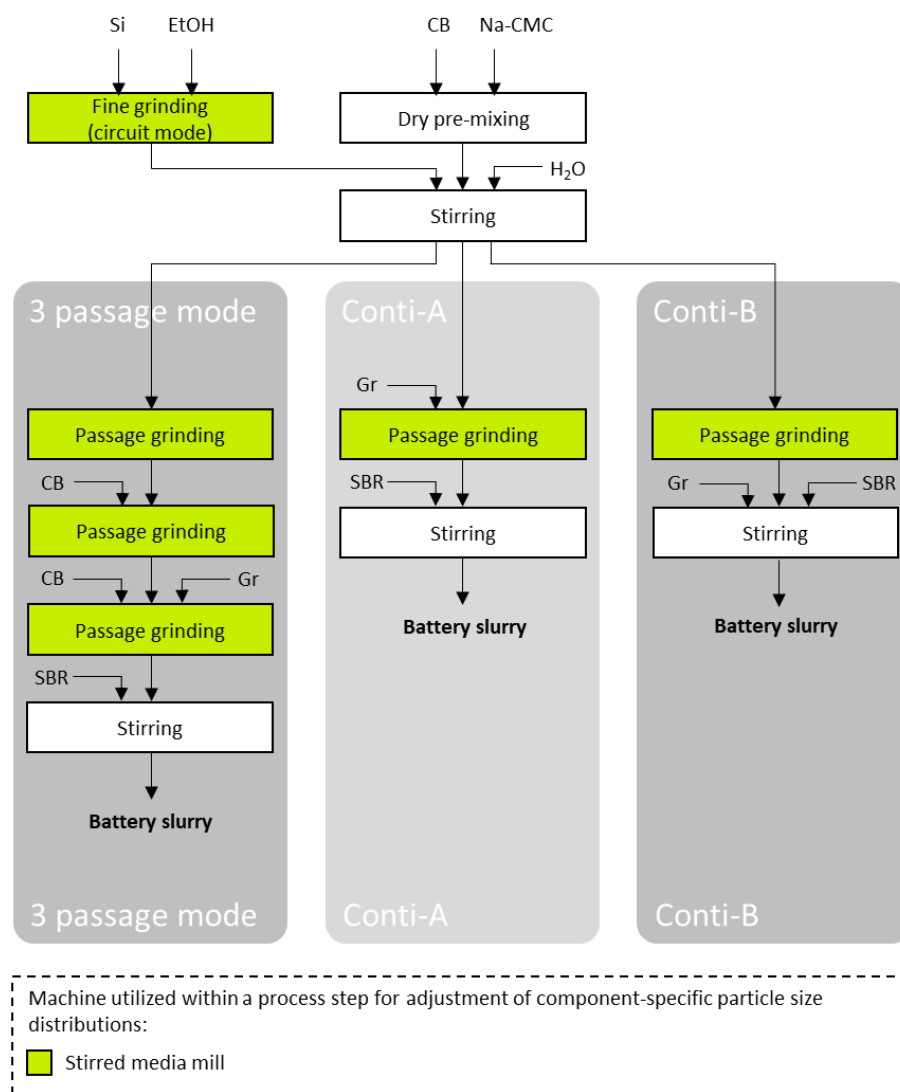


Figure 5. Process scheme for the production of battery slurries using the three different process routes: 3 passage mode, Conti-A, and Conti-B, based on a multicomponent comminution strategy within a stirred media mill.

2.4.2. Selective Characterization of Silicon-Carbon Black-Graphite Mixtures

Density separation was used as another method for the preparation of particulate mixtures [17]. Here, the difference in density of individual components is utilized to separate the particles. The very finely adjustable density of a sodium polytungstate salt solution (SPT solution) in the range of $1.0\text{--}3.1\text{ g}\cdot\text{cm}^{-3}$ [18] creates a sedimentation barrier for particles with lower density, while the heavy particles pass through the SPT solution and can thus be separated by centrifugation. For this, 4 mL of the SPT solution was first pipetted into a 15 mL Falcon tube, and then 1 mL of a diluted grinding sample ($c_{m,tot} = 0.01$) was carefully layered on top of the SPT solution through a syringe equipped with a thin needle. After centrifugation of the samples in a centrifuge with a swing-out rotor, both particle species are presently separated from each other so that they can then be pipetted out individually and analyzed by laser diffraction. In addition to the component-specific density difference, an important prerequisite for achieving a high separation quality with this method is, above all, the colloidal stability of both mixture components. Due to the formation of so-called heteroagglomerate structures consisting of both components with an overall higher density than the low-density material, even the light particles would sediment and thus reduce the separation efficiency.

In this work, for the preparation of a silicon-carbon black-graphite mixture, with stabilization of the carbon black and graphite particles by Na-CMC and after the dissolution of the silicon particles with 5 molar aqueous sodium hydroxide solution (stirred for min. 10 h at 50 °C), the separation of the carbon black and graphite particles was realized by using a 65 wt.% SPT solution with a density of $2.1 \text{ g}\cdot\text{cm}^{-1}$. Thus, sedimentation of the carbon black particles was effectively prevented, and that of the graphite particles was allowed. A schematic illustration of the procedure, as well as an exemplary analysis result for the separation of the carbon black and graphite particles out of the mixture in comparison to the previous measurement of the individual components, is shown in Figure 6.

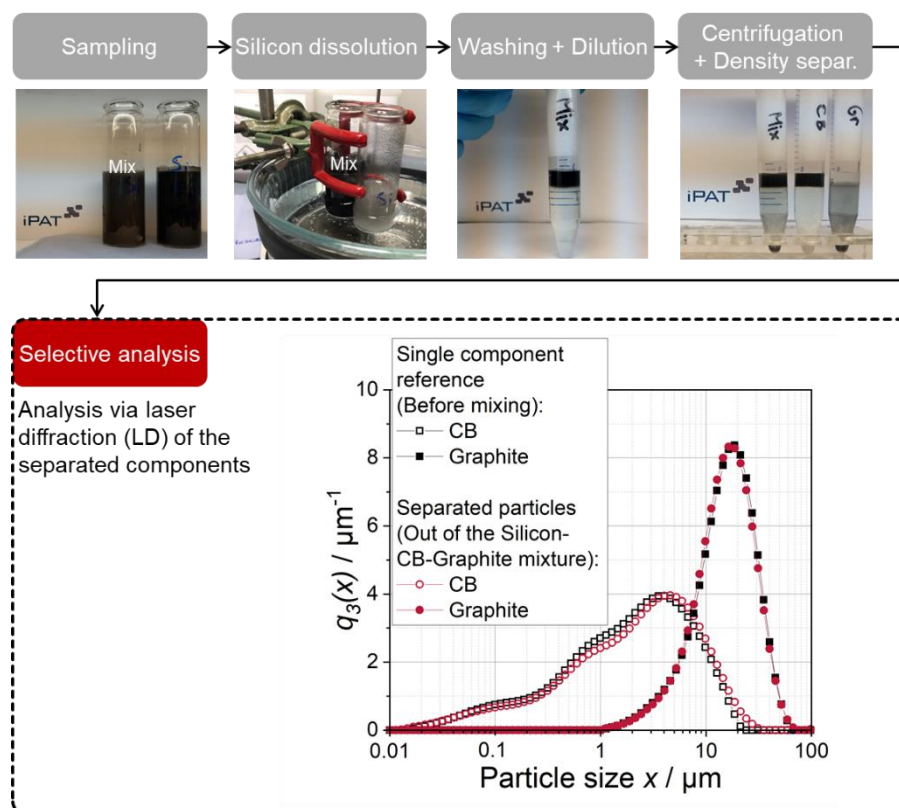


Figure 6. Scheme of the sample preparation to separate the carbon black (CB) and graphite particles from a silicon-CB-graphite mixture for a subsequent selective particle size analysis of both components by laser diffraction (LD).

2.5. Nanoindentation of Particles

In order to gain information about the particle strength of the different materials used in this work, nanoindentation characterization was carried out. The instrument used was the TI 980 TriboIndenter from Bruker Corporation, USA. The Flatpunch 50 (diameter: 50 μm) was used as an indenter tip. At least 40 particles per material were individually indented. The determined force at which the particle broke (breaking force) was related to the particulate cross-sectional area, which was previously identified with the optical unit of the device, in order to calculate the material-specific and particle size-dependent breakage strength.

2.6. Rheological Characterisation of Suspensions

For the evaluation of the rheological behavior of the battery slurries, suspension samples were characterized by rotational viscometry using the Kinexus pro from Malvern Panalytical Ltd., United Kingdom. For the analysis of the dynamic viscosity, the suspension was tempered to 20 °C before each measurement. The shear rate-dependent viscosity was then analyzed in the range of 0.01–500 s^{-1} using a cone-plate geometry.

2.7. Manufacturing of Silicon-Rich Anodes

After the battery slurry was prepared, it was further processed downstream to produce an electrode coating. A 10 μm thick copper foil (from Furukawa Electric Co., Japan), which was automatically unwound and rewound in the form of a coil during the process, was used as the substrate for the production of the electrode. For coating the copper foil with the suspension, the combined pilot-scale coating and drying machine Labco of Kroenert GmbH & Co KG, Germany, was used. The coater had a combined coating system with a comma-bar reversed-roll application system. The convective dryer unit had three separately controllable dryer segments of 2 m length each. For the production of the anode coatings in this work, a temperature of 65 °C and a diffuse inflow angle of the dryer air were chosen in the first two segments. In the last segment, a temperature of 100 °C and a direct inflow angle was used. The coating and drying speed was set to 2 $\text{m}\cdot\text{min}^{-1}$ (accordingly residence time of 3 min), and an aerial capacity of 2 $\text{mAh}\cdot\text{cm}^{-2}$ was adjusted via the variable distance of the doctor blade to the copper substrate. The final assembly of the produced electrode coil was performed manually with a cutting knife. The electrode sheets obtained were sealed in aluminum composite foil bags for storage under an argon atmosphere.

2.8. Characterization of Silicon-Rich Anodes

2.8.1. Electrochemical Testing

The electrode coatings were characterized in the PAT-Cell set-up from EL-CELL GmbH, Germany. The electrodes developed in the course of this work were used as an anode. For the counter-electrode, a lithium metal oxide-based cathode produced with a conventional formulation using the active material lithium nickel manganese cobalt oxide (NMC622 from BASF SE, Germany) was utilized to realize a full cell. The separator was double-layered using a combination of FS-5P Freudenberg Viledon FS 2226E from Freudenberg Filtration Technology GmbH & Co. KG, Germany, and Solupor 5P09B from Lydall Performance Materials Incorporated, United Kingdom. A liquid electrolyte was used to create an ionic transport between the electrodes. This consisted of ethylene carbonate and ethyl methyl carbonate mixture (mixing ratio 3:7) as well as the conducting salt lithium hexafluorophosphate with a concentration of 1 $\text{mol}\cdot\text{L}^{-1}$ (premixed from E-lyte Innovations GmbH, Germany). In addition, 2% vinylene carbonate and 10% fluoroethylene carbonate were added to the electrolyte as additives. After manual assembly of all cell components under an argon atmosphere inside a glovebox, the test cells were cycled under defined conditions.

The cells were charged and discharged with the use of a battery tester from Maccor Incorporated, USA. The selected voltage window ranged between 2.9 V and 4.2 V both during the formation and the subsequent C-rate test, as well as the subsequent long-term cycling. The determined capacity values for each battery cell were related to the coating mass of the electrodes used in order to obtain their specific capacity values. The C-rates used are shown in Table 2.

Table 2. Status, number of cycles, and C-rates during charge and discharge of the full cells for the evaluation of the electrochemical anode coating properties.

Status	Number of Cycles/–	Charge C-Rate/–	Discharge C-Rate/–
Formation	3	0.1	0.1
	3	0.1	0.1
C-rate test	3	0.1	0.3
	2	0.1	0.1
	3	0.1	0.5
	2	0.1	0.1
	3	0.1	1.0
	2	0.1	0.1
Cyclization (2 repetitions)	50	0.1	0.3
	2	0.1	0.1

2.8.2. Scanning Electron Microscopy

Scanning electron microscopy (SEM) was used to produce high-resolution secondary electron images of the electrode coating (top view and cross-section) and the particles inside it in order to gain a visual impression of the coating. The microscope used was the Helios G4 CX with DualBeam system from FEI Technologies Incorporated, USA.

3. Results

3.1. Investigation of the Feed Particle Strength

At the beginning of the investigations, the fracture-mechanical characterization of the particulate feed materials was carried out with the help of indentation tests. In each case, 40 particles of material were stressed in compression between a base plate and a movable, flattened indenter tip. Figure 7 shows the results of the five materials for which true fracture behavior was completely or, in the case of graphite, at least partially detectable.

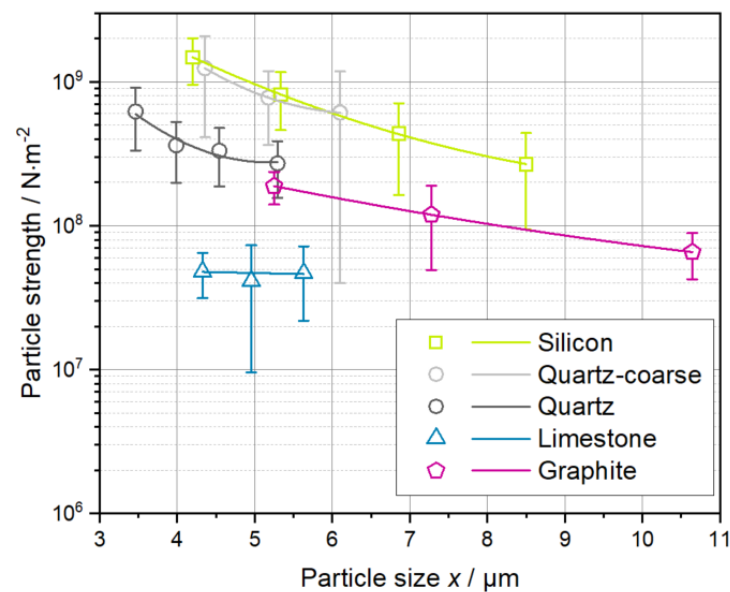


Figure 7. Particle strength as a function of particle size for five particle types investigated.

For all materials, an increase in the particle fracture strength with decreasing particle size can be observed. This characteristic behavior is independent of the material type and can be explained by the reduced number of defects in smaller particles [19].

When comparing the materials with each other, it is evident that silicon and the coarser quartz material (quartz-coarse) have almost identical particle fracture strengths for equivalent particle sizes. At a particle size of 5 μm , therefore, both materials exhibit a particle fracture strength of approx. $800 \text{ MN}\cdot\text{m}^{-2}$, which represents the highest value of all investigated materials.

In contrast, the particles of the finer quartz grade (quartz) show only a reduced particle fracture strength of approx. $300 \text{ MN}\cdot\text{m}^{-2}$. This result clearly shows that, in addition to the pure material property, the “history” of the material or, in other words, its intrinsic material structure, which may contain dislocations and initial cracks from more intensified previous milling processes, also plays a decisive role in the fracture behavior of the particles. Furthermore, it must be noted that the optical resolution reached its limit for the detection and size measurement of the single particles in the range of 3 to 5 μm . Thus, due to its high fineness, the incorrect detection of quartz agglomerates as individual particles could have contributed incorrectly to the determination of lower strength values.

With regard to the fracture strength values of the graphite particles, which can be as high as $200 \text{ MN}\cdot\text{m}^{-2}$ for 5 μm particles, a true fracture was only detectable in approx. 50% of the stressed particles. In the other cases, the material seemed to “slide away” under

the indenter tip when the pressure load was increased so that no measured value for the breaking strength could be identified. This finding can be explained by the intrinsic material structure of the layered graphite particles and the accompanying transverse shearing of individual graphite layers during particle loading.

The limestone particles exhibit the lowest detectable fracture strength. At a particle size of 5 μm , they have an average particle fracture strength of only approx. $41 \text{ MN}\cdot\text{m}^{-2}$.

In the case of the carbon black aggregates, no breakage signal was detectable during the measurement. Thus, although dislocation and local breakage of primary particle bridges occur by the indenter method, no significant interruption of the force-displacement curve could be detected, which would characterize particle breakage of hard materials. Therefore, the microscale carbon black aggregates appear to have a local strength that is below the detection limit of the method used. Hence, no curve could be plotted in Figure 7 for this material. However, we assume that the carbon black aggregates have the lowest strength of all the materials investigated in this study.

3.2. Basic Grinding Behavior of Stirred Media Mills during Grinding of Particulate Mixtures with Different Feed Particle Sizes

In order to analyze the influence of the component-specific feed particle size on the result of grinding material mixtures within a stirred media mill, basic experiments were carried out following our previous study [14]. Therefore, the two easily analyzable model materials, quartz (hard component) and limestone (soft component), were used. For the investigations, operating conditions of the stirred media mill were selected, which ensure an almost identical grinding of both components with identical feed particle size [14].

In Figure 8 the resulting component-specific particle sizes (red lines: grinding of material mixtures) are shown in dependency of the total specific energy input for the grinding of three different quartz-limestone mixtures and in comparison, to the single component grinding result (gray lines: quartz; blue lines: limestone).

Compared to the multicomponent grinding with very similar starting feed sizes (see Figure 8a), a considerable influence of the starting particle size ratio on the grindability of the quartz particles can be seen in the mixtures with pre-ground quartz (cf. Figure 8b). Thus, the finer quartz particles provided are not significantly ground at the beginning of the process. Only after the limestone particle size has been equalized with the quartz particle size the latter is also ground during further processing. Thus, the coarser limestone particles present in the mixture at the beginning of the process seem to apply a protective effect on the quartz particles. This protective effect is shown schematically in Figure 9.

Thus, during stirred media milling of mixtures in which hard but finer particles have been added, it can be assumed that no grinding progress is made with respect to this component until the other component also exhibits a similar particle size. This process window is shown in Figure 8 as a stable process window for the sequential grinding of several mixture components with fine hard particles.

In order to investigate this hypothesis in more detail, further investigations were undertaken with the particle size ratio of the components reversed. Here, the limestone particles were pre-ground to a median particle size $x_{50,3}$ of $0.55 \mu\text{m}$ and further ground after mixing with coarse quartz feed material. The results are shown in Figure 8c. When comparing the grinding progress with pre-ground limestone and with pre-ground quartz (cf. Figure 8b), no grinding progress can be observed for the limestone particles, even in the case of a finer limestone fraction presented at the beginning of the process. However, this already starts after a shorter process time of 10 min or a specific energy input $E_{m,tot}$ of approx. $420 \text{ kJ}\cdot\text{kg}^{-1}$ compared to the case of the mixture with pre-ground quartz (160 min, $4867 \text{ kJ}\cdot\text{kg}^{-1}$). Thus, although the quartz particles are still much coarser in the mixture at this stage ($x_{50,3} \approx 2 \mu\text{m}$), an initially reduced number of low-intensity stress events is consequently sufficient to further grind the softer limestone particles. In the further course of grinding, in contrast to the previous results with pre-ground quartz, there is no equalization of the particle sizes of the pre-ground limestone and the coarser quartz

noticeable. From a quartz particle size $x_{50,3}$ of $0.6 \mu\text{m}$, a constant particle size ratio of two is generated. According to Kwade [19], the capturing of multiple particles is very likely in this particle size range. At the same time, the particle-specific stress energy demand also decreases because the ratio of the provided stress energy of the grinding media related to the average captured particle mass and the stress intensity required for a particle breakage increases. Hence, it can be assumed that in the case of fine limestone particles, the transferable stress energy is sufficient on average to cause a fracture. Therefore, the fracture behavior of the particles is set according to their fracture-relevant material properties so that the material-specific grinding course of both components in the mixture follows the respective course of their individual material grinding course.

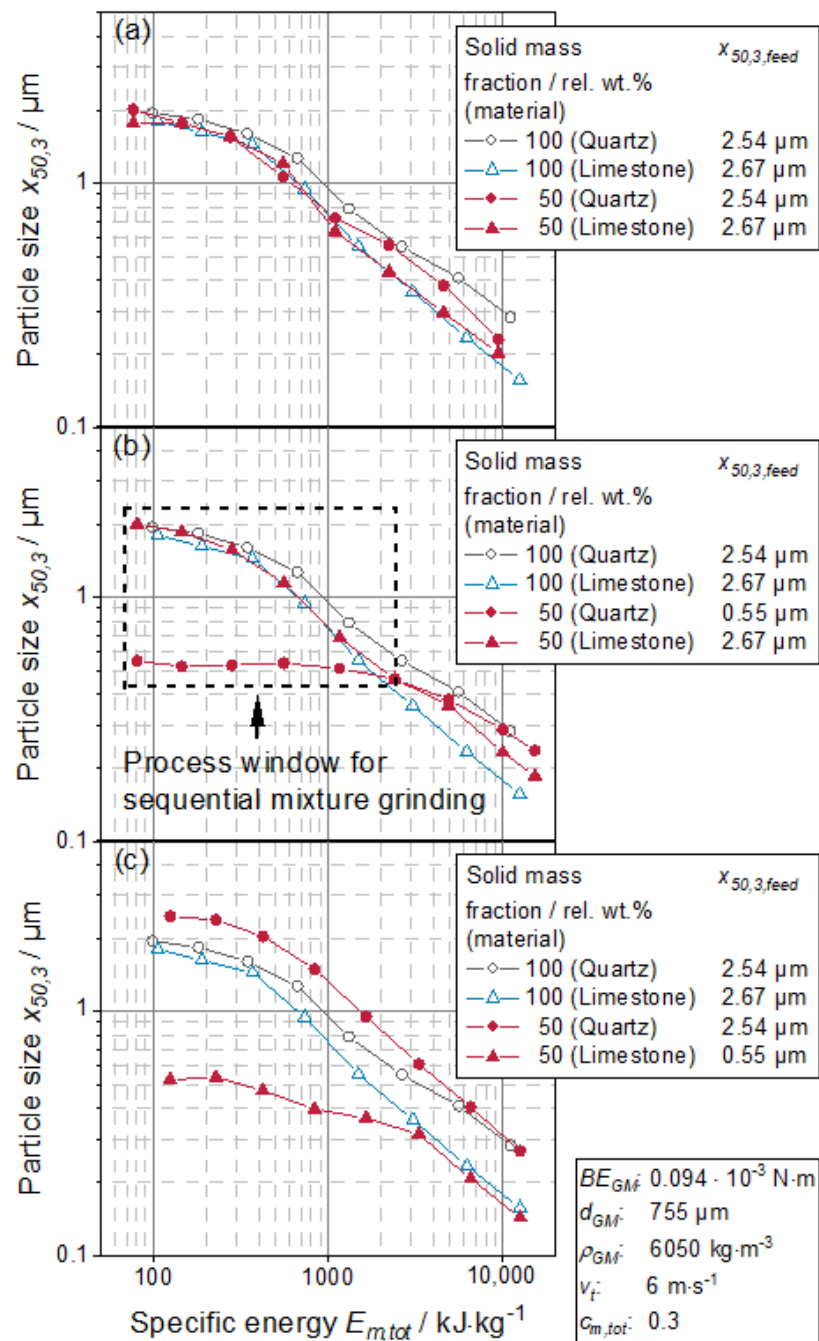


Figure 8. Influence of the initial particle size ratio of quartz and limestone on the component-specific grinding behavior with varied feed particle size $x_{50,3,feed}$ of both components.

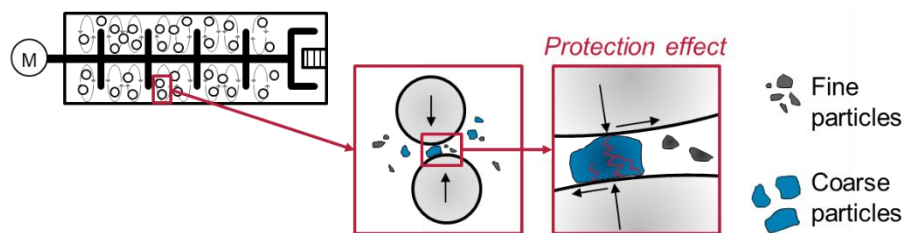


Figure 9. Schematic representation of the protection effect occurring during stirred media milling of mixtures with individual components of different sizes.

3.3. Targeted Preparation of Battery Slurries within a Stirred Media Mill

The resulting component-specific particle size distributions after silicon grinding and further processing of all components to a battery slurry within the reference process (cf. Figure 3) are shown in Figure 10, together with the particle size distributions of the respective feed materials. It can be seen that the hardest mixture component, silicon (cf. Figure 7), which starts with a median feed particle size $x_{50,3}$ around $20\ \mu\text{m}$, is present with the highest fineness in the system ($x_{50,3} = 200\ \text{nm}$). The most fragile material, carbon black, on the other hand, was not completely deagglomerated and, therefore, is widely distributed in the particle size range of $0.02\text{--}20\ \mu\text{m}$ ($x_{50,3} = 2.5\ \mu\text{m}$) after the dispersing process, which is advantageous from an application point of view [20]. In addition, the medium hard battery grade graphite ($x_{50,3} = 17\ \mu\text{m}$) was not broken but only distributed homogeneously in the suspension so that it has an identical particle size distribution to its feed material. Based on the investigated particle strength values (see Figure 7), the determined stable process window for stirred media milling of mixtures (see Figure 8) and the component-specific grinding target (see Figure 10), a clear option for the sequential multicomponent comminution of these three battery components can be identified with the following sequence of component addition: 1. silicon, 2. carbon black, 3. graphite.

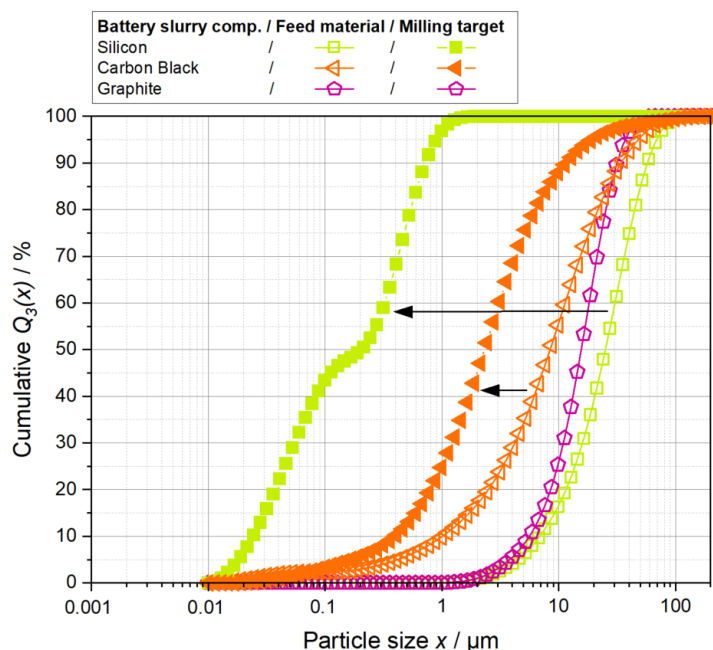


Figure 10. Particle size sum distributions $Q_3(x)$ of the three particulate feeds silicon, carbon black, and graphite and their milling targets for the production of silicon-containing anodes (gained by the reference process).

As it was already known that one to a few mill passages would be sufficient for the size reduction in the carbon black, the strategy was chosen to process all battery slurry components together within a passage-based operation of the mill. An exception was made

regarding the silicon particles, which needed to be ground to such fine values that the circuit operation of the mill was chosen upstream. Thus, this process step was identical to the silicon grinding step of the reference process.

In order to investigate the general comminution behavior of the three particulate components of the battery slurry, all three components were processed at their respective concentrations in the final coating suspension and within the final Na-CMC binder solution (without SBR). Since the single component grinding of silicon was planned upstream to this passage-based processing, the silicon particles were used as already ground particles in these experiments. In addition to the single component tests, carbon black—silicon and carbon black—graphite mixtures were also processed. The results of these experiments are summarized in Figure 11. For these results, a stirrer tip speed v_t of $4 \text{ m}\cdot\text{s}^{-1}$ ($SE_{GM} = 0.006\cdot 10^{-3} \text{ N}\cdot\text{m}$) and a constant volume flow \dot{V} through the mill of $11.4 \text{ L}\cdot\text{h}^{-1}$ was selected.

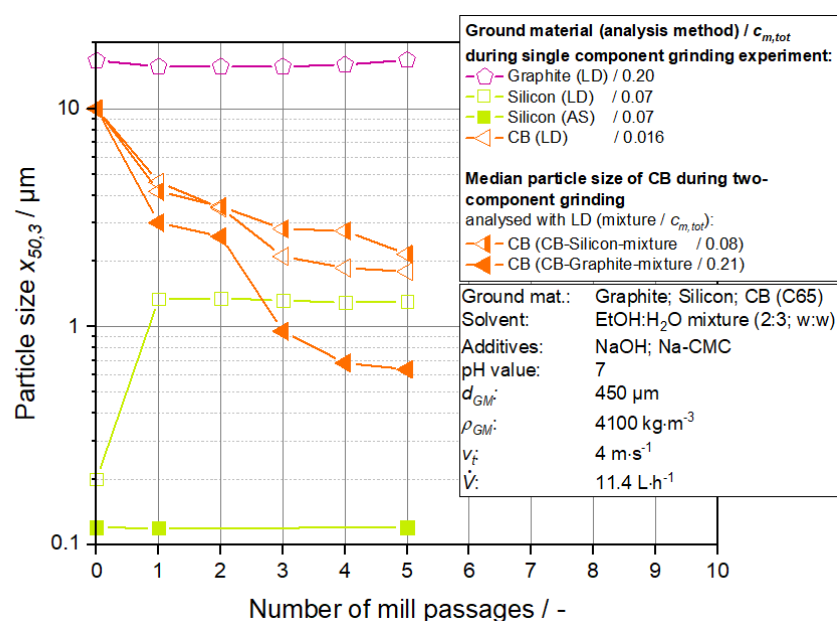


Figure 11. Median values of the three milled materials silicon, carbon black, and graphite during the processing of these individual materials as a function of the number of mill passages as well as for carbon black for the cases that it was processed together with silicon or graphite in a two-material mixture in each case.

In the case of a graphite—silicon mixture, no significant grinding can be detected within the considered process window of five passages. However, for silicon, a comparison of the results with laser diffraction and acoustic spectroscopy shows that a significant agglomeration of the particles has already occurred after one passage. In the further course of the process, the median value of the agglomerate size $x_{50,3}$ (LD) of $1.35 \text{ }\mu\text{m}$ also remains constant. However, it must be noted that the particle size analysis was based on a purely ethanolic silicon suspension before the first passage (0 passages) and that the silicon suspension was subsequently mixed with an aqueous binder solution using the binder Na-CMC.

It is also known that the partially deprotonated carboxyl group of the binder and the oxidized silicon surface react chemically [21], causing agglomeration of the silicon particles due to their high molecular weight, similar to flocculants. In contrast, Na-CMC increases the colloidal stability of carbon black particles in water and also ensures the formation of a homogeneous network between silicon and carbon black particles within coating suspensions for electrode production [21]. In the case of carbon black, in addition to single-material grinding, two-component processing with ground silicon particles or with graphite feed material was also investigated. The results show that in all three cases,

a significant size reduction in the carbon black takes place within five passages. Here, the individual material size reduction and the two-component processing with silicon particles ($x_{50,3}$ (AS) = 120 nm) proceed at almost identical levels, resulting in a reduction in the median value from 10 μm to about 2 μm at the end of the process. This result can be explained by the existing size ratios of the particulate components since the silicon particles are smaller than the carbon black agglomerates, and therefore the latter is exposed to the grinding media with the same frequency and intensity compared to the individual milling of the carbon black. However, it is interesting to note that multicomponent comminution with a carbon black—graphite mixture results in a more efficient comminution of the carbon black. In this case, the graphite particles increase the intensity and/or frequency of stresses acting on the carbon black agglomerates. Stadler et al. [22] described that for pigment deagglomeration with stirred media mills, the dispersing result for different applied stress energies of the grinding media could be represented by a predominantly stress-number-dependent correlation. Therefore, it is assumed in this context, with regard to the more efficient carbon black deagglomeration, that the graphite particles present in the two-component system provide additional shear forces acting on the carbon black. As described by Stadler et al. [22] and Kwade [19], for dispersing particles such as carbon black, the shear forces between the grinding media are relevant so that an increasing viscosity improves the shear stress acting on the carbon black agglomerates and, by that, improves the maximum possible fineness according to the model of Schilde et al. [23].

With regard to the median values determined for the individual components, these investigations show that the basic principle of passage-based processing in a stirred media mill is suitable for the production of a property-optimized battery slurry. However, it is also known from earlier work [20,24] that the carbon black particle size distribution, in particular, has significant influences on the coating suspension and final electrode properties. Therefore, in addition to considering the median value, the adjustment of the carbon black particle size distribution was also investigated in further experiments. Figure 12 presents the comparison between the reference process and the results for the passage-based single component comminution of the carbon black with the constant operation of the mill at a stirrer tip speed v_t of $4 \text{ m}\cdot\text{s}^{-1}$ ($SE_{GM} = 0.006\cdot 10^{-3} \text{ N}\cdot\text{m}$) and a volume flow \dot{V} through the mill of $11.4 \text{ L}\cdot\text{h}^{-1}$.

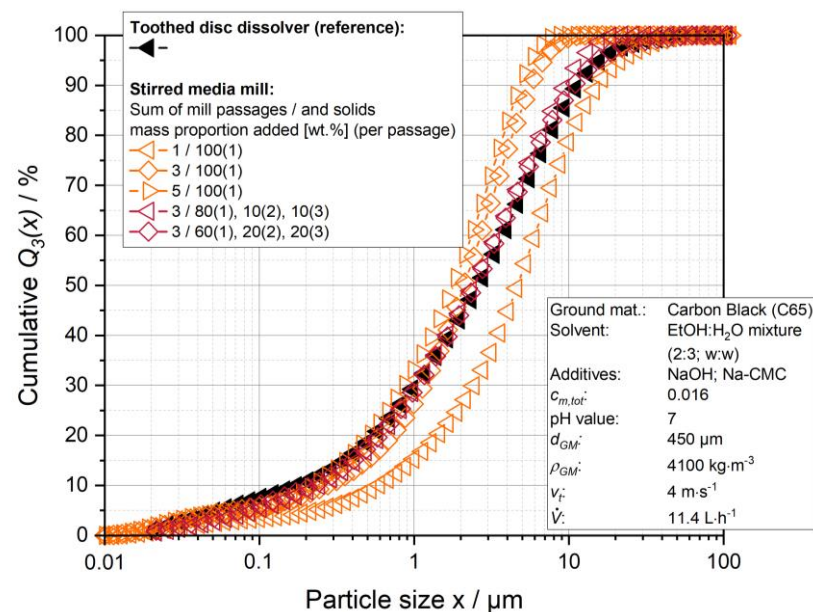


Figure 12. Particle size sum distributions $Q_3(x)$ of the deagglomerated conductive carbon black produced with the reference process in a toothed disc dissolver as well as with a stirred media mill under variation of the number of mill passages and the passage-dependent addition of the carbon black.

Firstly, the milling result was investigated with a single addition of the entire carbon black mass at the start of the process with respect to the one, three, or five passages, as well as the sequential addition of the carbon black within three passages. The latter dosing method provided a sequential addition of carbon black of 80/10/10 wt.% and 60/20/20 wt.% before the first, second, and third passages. The corresponding result of this sequential carbon black addition was then analyzed after the third passage. The results show that for the selected operating parameters, a single addition of the entire carbon black mass at the beginning of the process results in narrower particle size distributions compared to the reference process. However, for one passage, the maximum carbon black size is still higher than in the reference process and gets significantly smaller than in the reference process for three and five passages. For five passages, almost no further dispersing effect is detectable as the stress intensity is too small to further disperse the fine carbon black agglomerates. In contrast, with the constant operation of the stirred media mill and sequential addition of the carbon black mass, an almost identical particle size distribution is obtained after three passages compared to the reference. Here, the best agreement is achieved with a particle size distribution of the carbon black addition of 60/20/20 wt.%. For the subsequent investigations regarding the feasibility of the coating suspension production with a stirred media mill, this sequence was selected as a possible process variant, with the graphite also being added in the third passage (3 passage mode).

In order to reduce the number of passages required for the targeted size reduction in the carbon black agglomerates from three to one passage, a parameter study was also undertaken on the influence of the stirrer tip speed v_t and the product volume flow. For this purpose, the stirrer tip speed v_t was set to 4/5/6/7, and 8 $\text{m}\cdot\text{s}^{-1}$ and three volume flows \dot{V} of 6.6/8.8 and 11.4, $\text{L}\cdot\text{h}^{-1}$ were investigated. The previously used grinding media were kept constant. All resulting particle size distributions are shown in Figure A1 in the Appendix A.

Figure 13 illustrates the experimental results with the highest agreement compared to the reference process. Thus, with a slightly increased stirrer, tip speed v_t of 5 $\text{m}\cdot\text{s}^{-1}$ and corresponding increased stress energy of the grinding media SE_{GM} of $0.009\cdot 10^{-3}$ $\text{N}\cdot\text{m}$ and simultaneously reduced product volume flow \dot{V} of 8.8 $\text{L}\cdot\text{h}^{-1}$, an almost identical carbon black particle size distribution can be obtained in continuous single-passage operation. By reducing the product volume flow \dot{V} , the residence time distribution within the mill becomes broader, also resulting in a broader particle size distribution [19]. Moreover, by increasing SE_{GM} , a finer product is also obtained at the product outlet of the mill, so that, in contrast to the one-passage result in Figure 12, one continuous passage already leads to a sufficient fineness of the carbon black.

For the following investigations on coating suspension production with a continuously operated stirred media mill, these parameters were used, and two process variants were investigated, in which the graphite was added before (Conti-A) and after the continuous passage (Conti-B) through the stirred media mill. In order to obtain an overview of the investigated processes used for the production of the battery slurry in a stirred media mill, the schematic summary of the process strategies in Figure 5 should be looked at.

The different process variants for the targeted carbon black dispersion in a stirred media mill: three passage mode, Conti-A, and Conti-B, were investigated with regard to their suitability for battery slurry production. In contrast to the results of the single component grinding of the carbon black, mixtures were always processed in these investigations. Here, silicon, as well as carbon black, were always part of the mixture, and graphite was added at a process-dependent stage. In the three passage mode, graphite was added before the third passage, and in the continuous single-passage processes before (Conti-A) or after (Conti-B) the passage. The component-specific particle size distributions of the produced battery slurries are compared with the reference process in Figure 14. Due to the constant processing of silicon in the circuit grinding process upstream, only an exemplary sum distribution of this material was shown for a better overview.

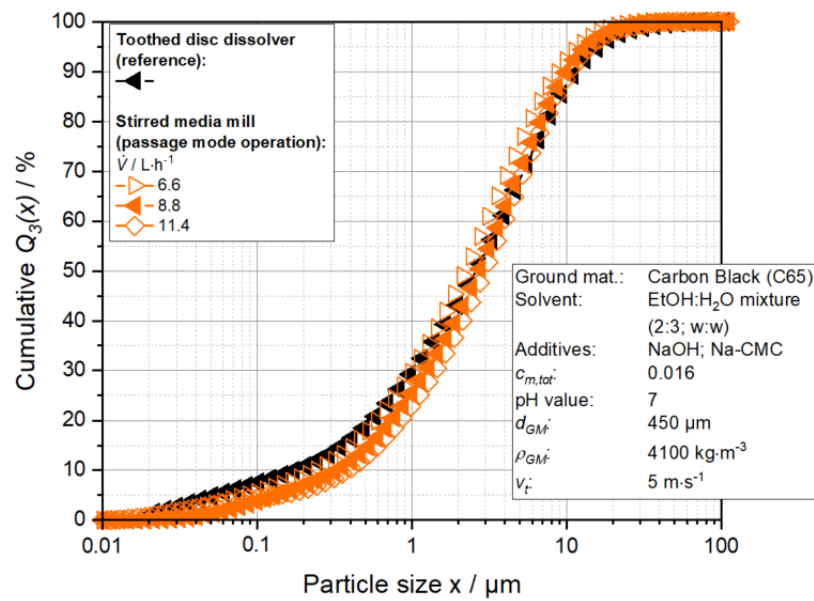


Figure 13. Comparison of resulting carbon black particle size distributions of the reference process and in a single-passage operation of a stirred media mill under variation of the product volume flow \dot{V} and at a stirrer tip speed v_t of $5 \text{ m}\cdot\text{s}^{-1}$.

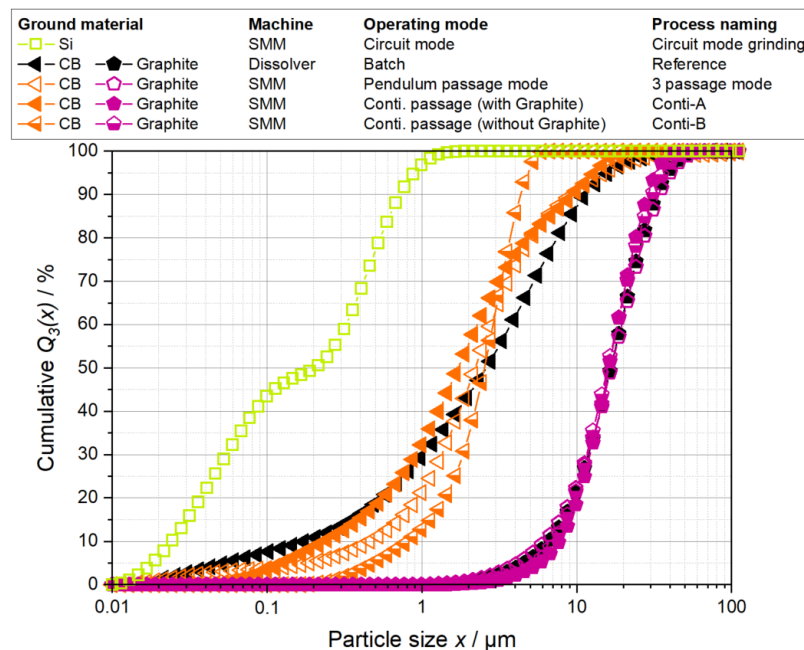


Figure 14. Particle size sum distributions $Q_3(x)$ of the particulate components of the battery slurry: silicon (exemplary) as well as carbon black and graphite, which were processed using four different processes.

For the graphite, the results show that its particle size distributions were almost identical for the four suspension types. This result shows that with sufficiently reduced stress energy of the grinding media SE_{GM} (3 passage mode: $SE_{GM} = 0.006 \cdot 10^{-3} \text{ N}\cdot\text{m}$; Conti-A: $SE_{GM} = 0.009 \cdot 10^{-3} \text{ N}\cdot\text{m}$), significant damage to the graphitic material structure can be avoided and the graphite is only suspended homogeneously. Comparing the obtained carbon black particle size distributions, similar median values in the range of $1.8\text{--}2.5 \mu\text{m}$ are obtained with all processes. Comparable particle size distributions with respect to the reference process are obtained with the Conti-A process and the three passage mode of the stirred media mill. Here, the presence of coarse graphite particles seems to have

a positive effect on the formation of a broader carbon black particle size distribution. As already discussed, shear forces between the graphite particles cause a more efficient dispersing of the carbon black fines (see Figure 11). However, the results also suggest that there appears to be an additional protective effect of the coarse graphite particles on the capturing and stressing of the carbon black agglomerates between the grinding media (see Figure 9, described protection effect). Thus, coarser carbon black agglomerates remain in the mixture compared to the Conti-B processing without the presence of the graphite particles. Thus, both effects support the formation of a broader particle size distribution. The very narrow particle size distribution resulting from the Conti-B process might be caused by the addition of the agglomerated silicon nanoparticles and, thus, by an increased viscosity which improved the shear forces acting on the carbon black particles.

The rheological behaviors of the suspensions were also of interest for the further processing of the produced battery slurries to electrode layers within the context of standardized processing downstream. Thus, the viscosity behavior influences the formation of the particulate electrode structure during the drying of coated wet films [25,26]. All prepared suspensions were characterized with respect to their rheological properties directly before the coating process (see Figure 15).

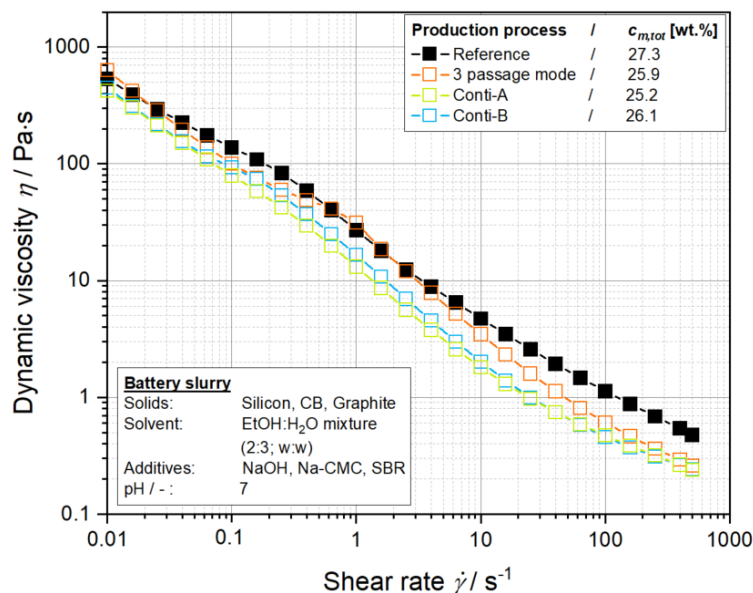


Figure 15. Dynamic viscosity of battery slurries produced by four different processes as a function of shear rate.

Figure 15 shows the dynamic viscosity of the coating suspensions as a function of the shear rate. All suspensions exhibit comparable shear-thinning flow behavior, which is required for a successful coating process. Especially in the low shear rate range, it is known for battery suspensions that the fractal dimensions of the carbon black aggregates play a major role in the formation of a certain viscosity level [27]. Thus, in combination with the findings shown in Figure 14, a similar structuring of carbon black for all produced battery slurries can be proven. In contrast to this, the suspensions produced with the process variants based on the stirred media mill exhibit a slightly lower viscosity in the higher shear rate range compared to the reference process. Within this shear rate range, the viscosity is mainly influenced by the total solids concentration $c_{m,tot}$ [27]. Therefore, small deviations regarding the $c_{m,tot}$ values of the single processes investigated may account for this effect (see Figure 15).

The obtained results of the selective particle size analysis and the viscosity investigations show that the process feasibility exists and that a property-optimized coating suspension can be obtained for all investigated multicomponent comminution processes.

3.4. Electrochemical Coating Properties Obtained by Different Slurry Production Processes

In addition to the process feasibility of the coating suspension production, the functionality of the manufactured coating product was also of particular interest. An optical impression of the prepared coatings is given from SEM images in the attachment (see Appendix A: Figures A2 and A3). In order to investigate the function of the coating, electrochemical tests were carried out with the prepared electrodes. The electrochemical results obtained for the full cells built are shown in Figures 16 and 17.

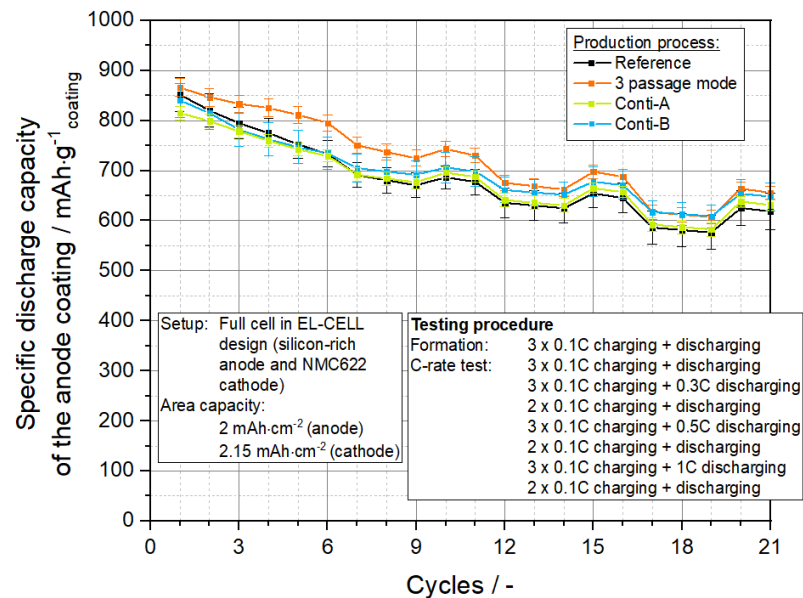


Figure 16. Specific discharge capacities of the silicon-rich anodes, which were produced by four different processes, as a function of the number of cycles during the formation and the C-rate test.

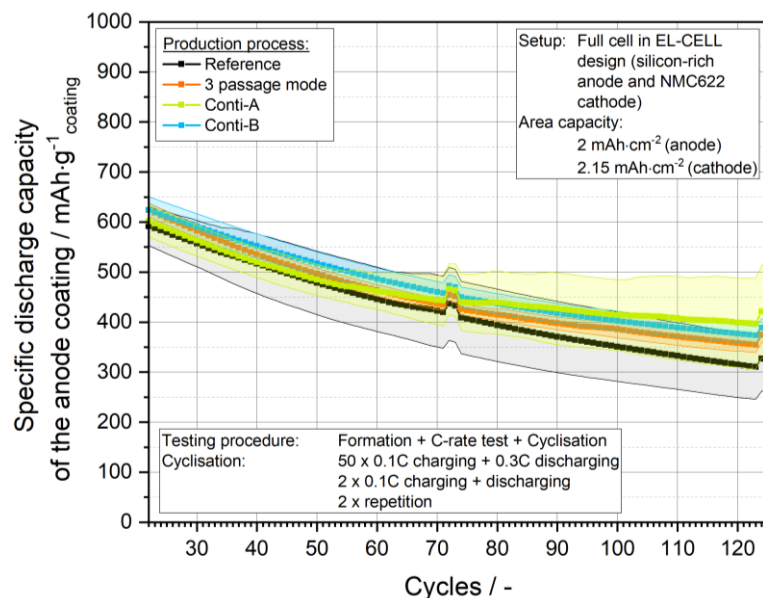


Figure 17. Specific discharge capacities of the silicon-rich anodes, which were produced by four different processes, as a function of the number of cycles during cycling (following the C-rate test, see Figure 16).

Both figures show the specific discharge capacity of the anode coating as a function of the number of charge-discharge cycles. The four anode types used here were named in line with the manufacturing procedure of the coating suspension since the subsequent

further processing was unchanged. At least four full cells were assembled and tested for each of the four production variants so that the curves shown correspond to the respective average value of the specific discharge capacity. Moreover, the standard deviations are also presented.

All anodes exhibit a comparable starting capacity in the range of 820–860 mAh·g⁻¹_{coating} regardless of the manufacturing process used (cf. Figure 16), which indicates basic comparability of the active material masses and their electrochemical accessibility in the electrodes. When comparing the curves during the cycling of the reference process with the three process variants based on the stirred media mill (see Figure 17), it is noticeable that the latter shows a slightly reduced decrease in specific discharge capacity in the range of higher cycle numbers. This could indicate a more homogeneous mixing of the components and, thus, of the electrode structure as a whole, which would result in a more reversible utilization of the electrochemically active silicon. The results clearly show that the general functionality of the prepared electrode coatings based on suspension processing in a stirred media mill exists and that the objective of this study could be achieved by the process strategy of multicomponent comminution. However, they also show that further optimization potential could be tapped in future work using this production technology, especially when using very fine active material particles that have to be finely dispersed and homogeneously embedded in an electrode structure.

4. Discussion

The presented results clearly show that both the procedural feasibility of coating suspension production within the stirred media mill and the functionality of the final electrode coatings exist. The sequential grinding of particulate coating components could be successfully implemented for this application based on the fundamental knowledge from basic experiments. The process was transferred from a discontinuous reference process using a toothed disc dissolver to the continuous single-passage operation of a stirred media mill. Figure 18 shows the plant diagram for the continuous process variant. With this process, an increase in throughput ($\dot{m} = 2.18 \text{ kg}\cdot\text{h}^{-1}$) by a factor of 5 could be achieved compared to the theoretical value of the reference process ($\dot{m}_{\text{theoretical}} = 0.44 \text{ kg}\cdot\text{h}^{-1}$), whereby a further increase in throughput, taking into account a constant mill size, should be possible by improving the pump performance and the accompanying increase in the product volume flow with simultaneous adjustment of the mill operating parameters. In the process developed, however, continuous dosing of the components upstream of the mill and also continuous mixing of the SBR binder were initially omitted. In the future, these process steps should also be able to be reproduced continuously with the appropriate plant dosing technology or could be converted to quasi-continuous operation by alternately feeding the mill with several feed tanks. The fine grinding of the silicon, on the other hand, was not integrated into the continuous operation of the stirred media mill, just as in the case of the discontinuous reference process, because the single-passage operation was rated as not suitable due to the required silicon fineness.

The developed process represents a combination of silicon grinding in circuit mode and subsequent single passage processing of the other coating components. Hence, it can also be realized with just one mill (as shown in Figure 4). The advantages (+) and disadvantages (−) of this process for the production of silicon-containing electrodes, where fine silicon particles need to be incorporated into the electrode structure, are as follows:

- + The use of inexpensive silicon educts in the micrometer range is possible (e.g., silicon wafer breakage or cutting dust from the semiconductor industry).
- + Efficient de-agglomeration when using silicon powders with an aggregate structure
- + Continuous production of the coating suspension
- + High energy density
- + High mixing intensity and, thus, higher homogeneity of the product
- + High throughput
- + Very good scalability of the process

- + High flexibility of the process, as the grinding media (size, density, filling degree of the mill), circumferential stirrer speed, volume flow, etc., can be adjusted to each other.
- The height of the maximum applicable stress energy is limited by the fact that the breakage of the graphite particles needs to be avoided.
- For mixing very fragile components into the slurry, the minimum applicable stress-energy in the mill might be too high if breakage must be avoided.
- Good knowledge about the process-material-property relationship is needed.
- The concentration of slurries is restricted

The solids concentration $c_{m,tot}$ of the coating suspension with 0.26 realized in this study so far represents a comparatively low value so there is still a need for further optimization with regard to economic efficiency. However, due to the widespread use of stirred media mills in the production of dispersion paints for the comminution of fillers and pigments with high solids contents of up to 0.7 [28], this potential clearly exists. In addition, current mill developments for the processing of high-viscosity products [1,29] could also be useful for economic optimization. Furthermore, combined processes between continuously operated stirred media mills, which are used for the adequate incorporation of the submicron components silicon and carbon black into the binder matrix, and extruders, which increase the maximum achievable solids concentration [13,30], for example, during the final addition of graphite, are also conceivable.

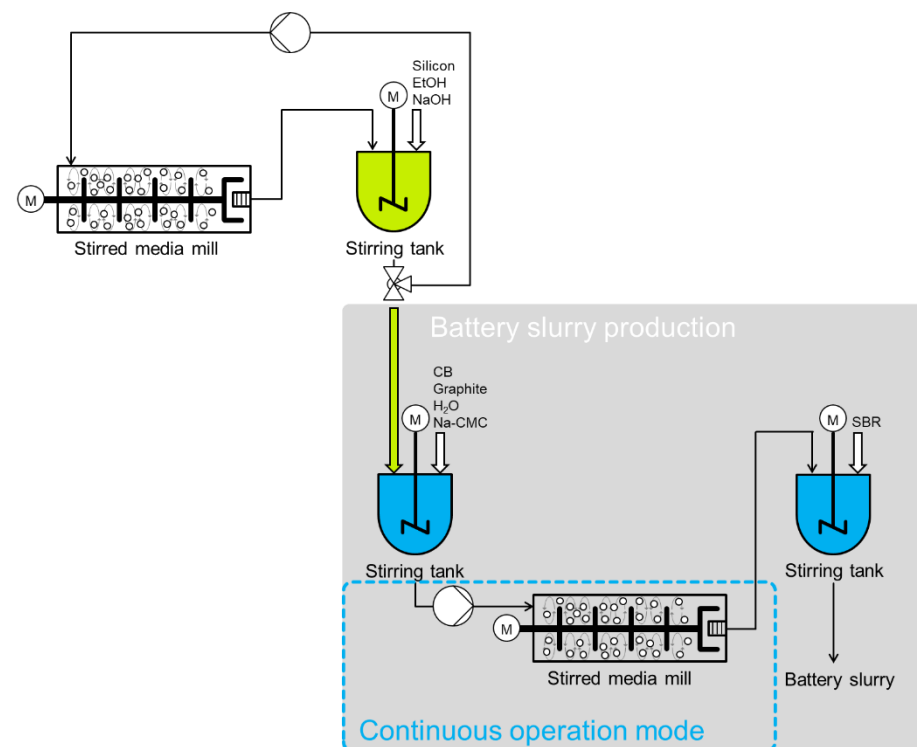


Figure 18. Plant diagram for the possible continuous operation of a stirred media mill (corresponding to the process variant: Conti-A) in the production of a battery slurry (area highlighted in grey).

5. Conclusions

The findings of this study clearly demonstrate that targeted particle size distributions of specific mixture components can be reached by stirred media milling and a multicomponent comminution approach.

Based on fundamental experiments, the sequence of component addition was elucidated as a key parameter. It needs to be chosen based on the component-specific particle strength and its grinding behavior as well as on the grinding target for each component. Especially if fine hard particles need to be ground together with weaker coarse particles (e.g., agglomerates), a stable process window can be reached due to a protection effect

caused by the coarser particles, which limits the transferable stress energy of colliding grinding beads on the fine particles. Therefore, the size of the fine hard particles stays constant as long as the other particulate mixture component reaches an equal particle size.

The transferability of the developed process strategy for multicomponent comminution was demonstrated within the scope of application-oriented investigations. The processed battery slurry contained three particulate components: silicon, carbon black, and graphite. Compared to a discontinuous, multistage reference process in a toothed disc dissolver, the processing of the mixture could be realized finally within only one continuous mill passage, whereby the circuit mode grinding of the silicon was realized upstream. The produced battery slurries were further processed to silicon-rich anode coatings, which were tested in full cells afterward. The results showed comparable electrochemical properties of the silicon-rich anodes, whereby the electrodes derived from a milling process showed slightly higher cycling stability. It should be mentioned here that in the case of using silicon aggregates in future work, which only need to be dispersed, the integration of the dispersion step by adding an additional continuous mill passage upstream could be investigated as a promising possibility.

Furthermore, these application-related investigations also showed a new effect in the joint processing of the battery grade graphite and the conductive additive carbon black. This resulted in a more efficient dispersing of the carbon black aggregates due to additional shear processes between the graphite particles. These additional stress events, which in the case of the carbon black aggregates have a comminution effect, could also be of interest for other applications. An example of this would be the multicomponent comminution of so-called hard filler and a soft color pigment in the production of dispersion paints [12]. The applicability of this process technology for this case could also be further explored in future work.

Finally, these results demonstrate that the selective particle size analysis used is a powerful tool for the accurate and flexible transfer of mixing processes from one machine to another. However, the exact preparation strategy for the samples depends to a large extent on the properties (e.g., solubility or density) of the particulate mixture components and needs to be adapted, therefore, to the specific mixture system.

Author Contributions: Conceptualization, M.N., J.M. and C.N.; methodology, M.N. and J.M.; software, J.M.; validation, M.N. and J.M.; formal analysis, M.N., J.M., K.L. and X.X.; investigation, M.N., C.N., K.L. and X.X.; resources, M.N.; data curation, M.N.; writing—original draft preparation, M.N.; writing—review and editing, J.M., S.B.-F. and A.K.; visualization, M.N.; supervision, S.B.-F. and A.K.; project administration, A.K. and S.B.-F.; funding acquisition, S.B.-F. and A.K. All authors have read and agreed to the published version of the manuscript.

Funding: This research was funded by the German Federal Ministry of Education and Research (BMBF), grant number 03XP0035F.

Acknowledgments: We thank our colleagues Stephanie Michel for the nanoindentation analysis, Bogdan Semenenko for the SEM analysis, and Erik Kariger for his maintenance support.

Conflicts of Interest: The authors declare no conflict of interest.

Appendix A

Within this study stirred media milling was used as a dispersing process for carbon black agglomerates. In order to reduce the number of necessary mill passages for the targeted dispersion of the carbon black agglomerates to one passage, a parameter study was conducted on the influence of the stirrer tip speed v_t and the product volume flow \dot{V} . For this purpose, the stirrer tip speed v_t was varied to 4/5/6/7 and 8 $\text{m}\cdot\text{s}^{-1}$ and volume flow rates \dot{V} of 6.6/8.8 and 11.4 $\text{L}\cdot\text{h}^{-1}$ were investigated. The dispersing results are presented in Figure A1.

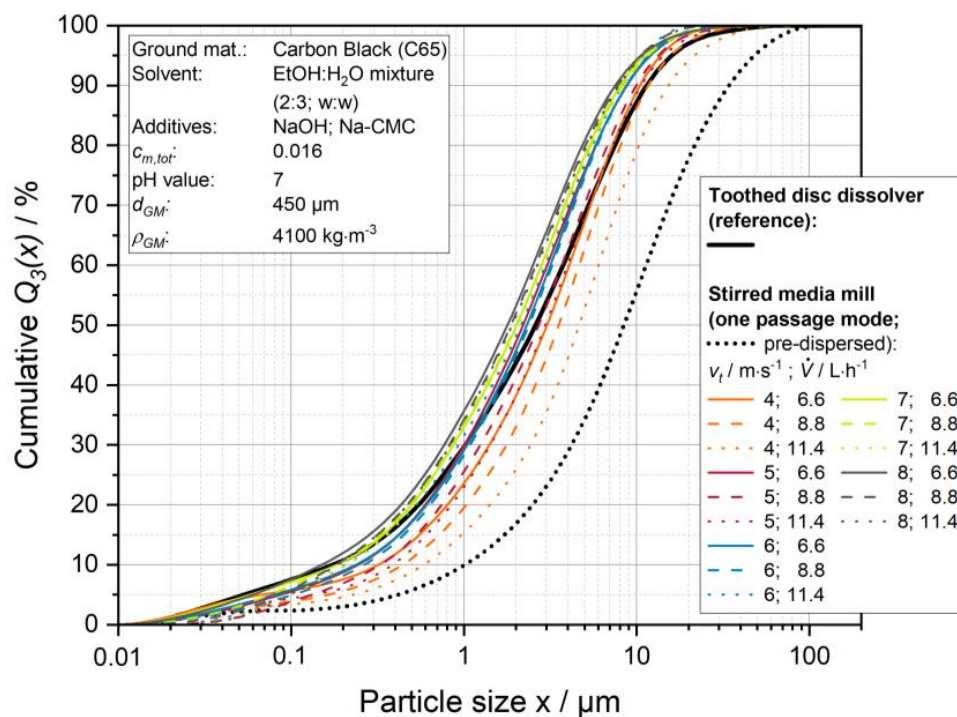


Figure A1. Comparison of resulting carbon black particle size distributions of the reference process and in a one- passage operation of a stirred media mill under variation of the product volume flow \dot{V} as well as the stirrer tip speed v_t .

An optical impression of the prepared **electrode** coatings is given in Figures A2 and A3.

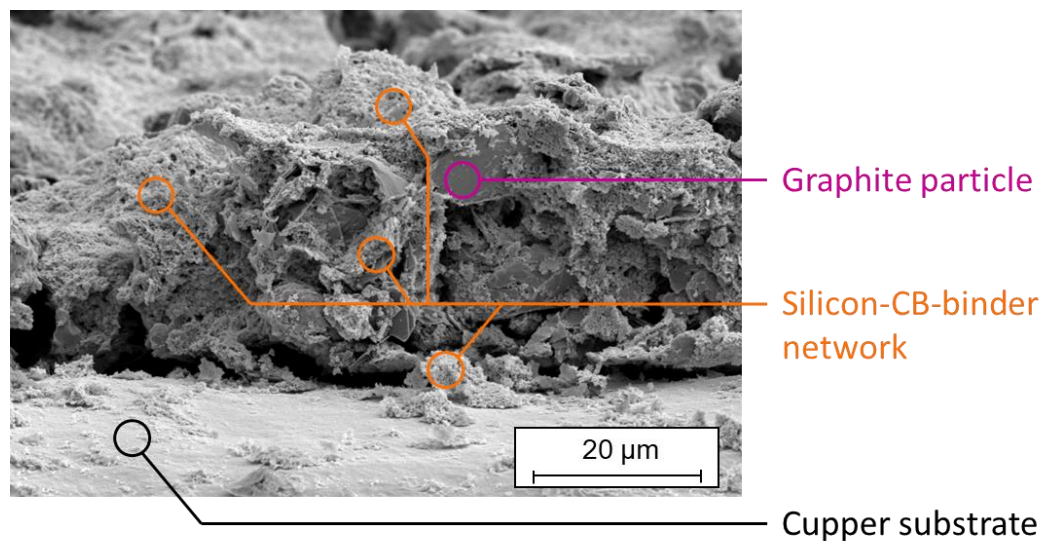


Figure A2. Cross-section of an exemplary silicon-rich anode (area capacity: $2 \text{ mAh}\cdot\text{cm}^{-2}$).

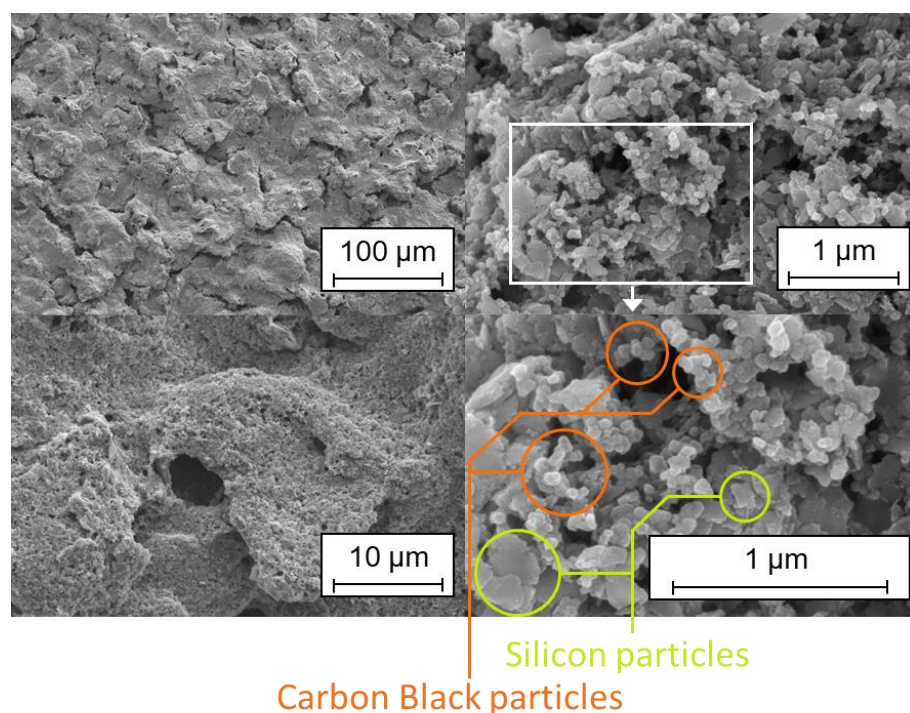


Figure A3. Top view of an exemplary silicon-rich anode (area capacity: $2 \text{ mAh}\cdot\text{cm}^{-2}$) with four different resolution levels.

References

1. Kern, N. Hoher Durchsatz und maximale Prozesssicherheit. *CITplus* **2019**, *22*, 36–38. [[CrossRef](#)]
2. Flach, F.; Breitung-Faes, S.; Kwade, A. Fine Grinding of Organic Materials in Stirred Media Mills: Determination of Advantageous Formulations and Process Parameters. *Chem. Ing. Tech.* **2016**, *88*, 850–856. [[CrossRef](#)]
3. Flach, F.; Fries, L.; Kammerhofer, J.; Hesselbach, J.; Finke, B.; Schilde, C.; Niederreiter, G.; Palzer, S.; Heinrich, S.; Kwade, A. Optimization of aqueous microgrinding processes for fibrous plant materials. *Adv. Powder Technol.* **2019**, *30*, 2823–2831. [[CrossRef](#)]
4. Reindl, A.; Aldabergenova, S.; Altin, E.; Frank, G.; Peukert, W. Dispersing silicon nanoparticles in a stirred media mill—investigating the evolution of morphology, structure and oxide formation. *Phys. Status Solidi (a)* **2007**, *204*, 2329–2338. [[CrossRef](#)]
5. Obrovac, M.N.; Christensen, L. Structural Changes in Silicon Anodes during Lithium Insertion/Extraction. *Electrochem. Solid-State Lett.* **2004**, *7*, A93. [[CrossRef](#)]
6. Liu, X.H.; Zhong, L.; Huang, S.; Mao, S.X.; Zhu, T.; Huang, J.Y. Size-Dependent Fracture of Silicon Nanoparticles during Lithiation. *ACS Nano* **2012**, *6*, 1522–1531. [[CrossRef](#)]
7. Hou, X.; Zhang, M.; Wang, J.; Hu, S.; Liu, X.; Shao, Z. High yield and low-cost ball milling synthesis of nano-flake Si@SiO₂ with small crystalline grains and abundant grain boundaries as a superior anode for Li-ion batteries. *J. Alloys Compd.* **2015**, *639*, 27–35. [[CrossRef](#)]
8. Leblanc, D.; Hovington, P.; Kim, C.; Guerfi, A.; Bélanger, D.; Zaghbi, K. Silicon as anode for high-energy lithium ion batteries: From molten ingot to nanoparticles. *J. Power Sources* **2015**, *299*, 529–536. [[CrossRef](#)]
9. Nguyen, B.; Chazelle, S.; Cerbelaud, M.; Porcher, W.; Lestriez, B. Manufacturing of industry-relevant silicon negative composite electrodes for lithium ion-cells. *J. Power Sources* **2014**, *262*, 112–122. [[CrossRef](#)]
10. Nilssen, B.E.; Kleiv, R.A. Silicon Powder Properties Produced in a Planetary Ball Mill as a Function of Grinding Time, Grinding Bead Size and Rotational Speed. *Silicon* **2020**, *12*, 2413–2423. [[CrossRef](#)]
11. Ashuri, M.; He, Q.; Shaw, L.L. Silicon as a potential anode material for Li-ion batteries: Where size, geometry and structure matter. *Nanoscale* **2016**, *8*, 74–103. [[CrossRef](#)] [[PubMed](#)]
12. Gysau, D. *Füllstoffe: Grundlagen und Anwendungen*, 2nd ed.; Technologie des Beschichtens, Vincentz Network: Hannover, Germany, 2006.
13. Dreger, H.; Bockholt, H.; Haselrieder, W.; Kwade, A. Discontinuous and Continuous Processing of Low-Solvent Battery Slurries for Lithium Nickel Cobalt Manganese Oxide Electrodes. *J. Electron. Mater.* **2015**, *44*, 4434–4443. [[CrossRef](#)]
14. Nöske, M.; Li, K.; Brüning, K.; Breitung-Faes, S.; Kwade, A. Impact of stress conditions on stirred media milling of a two component mixture. *Miner. Eng.* **2020**, *146*, 106100. [[CrossRef](#)]
15. Nöske, M.; Breitung-Faes, S.; Kwade, A. Electrostatic Stabilization and Characterization of Fine Ground Silicon Particles in Ethanol. *Silicon* **2019**, *11*, 3001–3010. [[CrossRef](#)]
16. Kwade, A. A Stressing Model for the Description and Optimization of Grinding Processes. *Chem. Eng. Technol.* **2003**, *26*, 199–205. [[CrossRef](#)]

17. Peppersack, C.; Kwade, A.; Breitung-Faes, S. Selective particle size analysis in binary submicron particle mixtures using density dependent differential sedimentation. *Adv. Powder Technol.* **2021**, *32*, 4049–4057. [[CrossRef](#)]
18. Gregory, M.R.; Johnston, K.A. A nontoxic substitute for hazardous heavy liquids—Aqueous sodium polytungstate ($3\text{Na}_2\text{WO}_4 \cdot 9\text{WO}_3 \cdot \text{H}_2\text{O}$) solution (Note). *N. Z. J. Geol. Geophys.* **1987**, *30*, 317–320. [[CrossRef](#)]
19. Kwade, A. *Zerkleinern und Dispergieren mit Rührwerkskugelmühlen*, 6th ed.; 2019. Available online: <https://gvt.org/Kurse/Archiv/Zerkleinern+und+Dispergieren+mit+R%C3%BChrwerkskugelm%C3%BChlen+2021.html> (accessed on 15 October 2022).
20. Haselrieder, W.; Ivanov, S.; Tran, H.; Theil, S.; Froböse, L.; Westphal, B.G.; Wohlfahrt-Mehrens, M.; Kwade, A. Influence of formulation method and related processes on structural, electrical and electrochemical properties of LMS/NCA-blend electrodes. *Prog. Solid State Chem.* **2014**, *42*, 157–174. [[CrossRef](#)]
21. Mazouzi, D.; Karkar, Z.; Hernandez, C.R.; Manero, P.J.; Guyomard, D.; Roué, L.; Lestriez, B. Critical roles of binders and formulation at multiscales of silicon-based composite electrodes. *J. Power Sources* **2015**, *280*, 533–549. [[CrossRef](#)]
22. Stadler, R.; Polke, R.; Schwedes, J.; Vock, F. Naßmahlung in Rührwerksmühlen. *Chem. Ing. Tech.* **1990**, *62*, 907–915. [[CrossRef](#)]
23. Schilde, C.; Kampen, I.; Kwade, A. Dispersion kinetics of nano-sized particles for different dispersing machines. *Chem. Eng. Sci.* **2010**, *65*, 3518–3527. [[CrossRef](#)]
24. Bockholt, H.; Haselrieder, W.; Kwade, A. Intensive powder mixing for dry dispersing of carbon black and its relevance for lithium-ion battery cathodes. *Powder Technol.* **2016**, *297*, 266–274. [[CrossRef](#)]
25. Du, Y.F.; Zang, Y.H. Study of Latex Migration Mechanism during Coating Consolidation. *Adv. Mater. Res.* **2011**, *295–297*, 83–87. [[CrossRef](#)]
26. Westphal, B.G.; Kwade, A. Critical electrode properties and drying conditions causing component segregation in graphitic anodes for lithium-ion batteries. *J. Energy Storage* **2018**, *18*, 509–517. [[CrossRef](#)]
27. Bockholt, H.; Indrikova, M.; Netz, A.; Golks, F.; Kwade, A. The interaction of consecutive process steps in the manufacturing of lithium-ion battery electrodes with regard to structural and electrochemical properties. *J. Power Sources* **2016**, *325*, 140–151. [[CrossRef](#)]
28. Rähse, I.W. Product Design of Disperse Solids by Breaking up Materials. *Chem. Ing. Tech.* **2011**, *83*, 598–611. [[CrossRef](#)]
29. Mütze, T. Comminution Technology in Times of SOPs and Apps. *Chem. Ing. Tech.* **2018**, *90*, 2004–2010. [[CrossRef](#)]
30. Dreger, H.; Haselrieder, W.; Kwade, A. Influence of dispersing by extrusion and calendering on the performance of lithium-ion battery electrodes. *J. Energy Storage* **2019**, *21*, 231–240. [[CrossRef](#)]